Investigation on an air solar-driven open sorption system for comfort cooling

Elsabet Nielsen, corresponding author
Department of Civil Engineering, Technical University of Denmark
Brovej 118, 2800 Kgs. Lyngby, Denmark
ean@byg.dtu.dk

Sonja Becker-Hardt
Heliac ApS
Savsvinget 4D, 2970 Hørsholm, Denmark
sbh@heliac.dk

Gerald Englmair
Department of Civil Engineering, Technical University of Denmark
Brovej 118, 2800 Kgs. Lyngby, Denmark
gereng@byg.dtu.dk

Weiqiang Kong
Department of Civil Engineering, Technical University of Denmark
Brovej 118, 2800 Kgs. Lyngby, Denmark
weiko@byg.dtu.dk

Simon Furbo
Department of Civil Engineering, Technical University of Denmark
Brovej 118, 2800 Kgs. Lyngby, Denmark
sf@byg.dtu.dk

https://doi.org/10.1016/j.solener.2021.11.018

Abstract

An air solar-driven open sorption system for comfort cooling is investigated experimentally in an indoor test facility. The main components of the system are a solar dehumidifier and a cold storage with desiccant. One operation cycle is 36 hours. On the first day of the operation cycle, the solar dehumidifier is charged. At night the cold storage is charged and on day two, the cold storage is discharged. A material investigation is undertaken to find the most suitable desiccant for both components, including samples of different silica gels and zeolites. The scope of this work is to determine the usability and the performance of the system. The usability of the system is addressed by an investigation of the climatic conditions of fourteen different locations. It is shown that a small porous silica gel is the best desiccant for both the solar dehumidifier and cold storage, that the system can work well in eight of the investigated climates, and that the system can supply cool, dry air for comfort cooling of buildings.

Keywords: solar comfort cooling, silica gel water as working pair, sorption material investigation, climate investigation

1. Introduction and background

The energy demand for cooling/air-conditioning is increasing continuously (Kalkan et al., 2012). The reason is growing thermal loads, changing building architecture modes, rising temperatures and the phenomenon of heat islands in urban areas (Oke et al., 1991, Grignon-Masse et al., 2011), and especially increasing occupants indoor comfort demand resulting in higher electricity demand notably during peak loads (Ghafoor and Munir, 2015).

The most widespread technology of commercial air-conditioners, the electrical powered vapor compression machines face the paradox that the more air-conditioners installed in a city, the more heat is released to urban atmosphere, and the more ambient air temperature increases. This phenomenon, contributing to the co-called urban heat islands, makes air temperature of large cities increase by as much as 10 K compared to countryside (Santamouris et al., 2001). The negative influences are increased cooling demand in buildings and reduced performance efficiency of traditional air-conditioners. Both effects unfortunately add to each other, leading to increased peak electricity demand for cooling purposes and an augmented risk of grid failures in summer peak hours (Pons et al., 2012, Bongs et al., 2014)

In 2016, air-conditioning accounted for nearly 20% of the total electricity demand in buildings worldwide and consumption is growing faster than any other energy use in buildings. If this development continues, the demand for space cooling will almost triple by 2050 to 6200 TWh corresponding to 30% of the total electricity use in buildings (Jakob, 2020).

Solar cooling technologies are beneficial particularly due to strong correlation between supply of the solar resource and demand for cooling during daytime, while efficient heat storage technique can also fully or partially cover cooling demand during nighttime (Grossman, 2002, Ghafoor and Munie, 2015, IEA, 2012). Thus, solar thermal cooling technology can reduce electric grid load at peak cooling demand periods by partially or fully replacing electricity needed for conventional vapor compression chillers or room air-conditioners (RAC) (Ghafoor and Munir, 2015).

Solar thermally driven cooling technology is classified into two main categories: closed cycles for chilled water systems and open cycles for direct treatment of air for temperature and humidity control (Ghafoor and Munir, 2015).

Solar cooling systems are generally comprised of three sub-systems: the solar energy conversion systems, refrigeration systems, and the cooling distribution systems. The appropriate cycle in each application depends on many factors such as the cooling demand, power, the temperature levels of the building in question, the environment etc. The solar thermal-driven air conditioning cycle can be based on absorption cycle, adsorption cycle, ranking cycle, desiccant cooling cycle, or ejector cycle (Abdulateef et al., 2009, Boopathi and Shanmugam, 2012).

The components of the system comprise of: buffer storage to store heat for extended hours of use, heat distribution system for supply to sorption chiller, thermally driven cooling machine to produce chilled water, cooling tower (dry or wet type) to reject heat to the ambient, air conditioning system for cold distribution, auxiliary (backup) heating system (electric, gas or oil boiler) for periods with scarce or no radiation, pumps to regulate the flow rate and controllers for automatic operation of the system (Ghafoor and Munir, 2015).

Open sorption cycles are simpler than closed sorption cycles, as they do not require condenser, evaporator, water storage reservoir, and maintenance of system pressure and complex control strategy (Yu et al., 2013).

Experiments and simulation have shown that the silica gel-water adsorption cycle is well suited to near-environmental-temperature heat sources and small regeneration temperature lifts (Boelman et al., 1995).

Desiccant evaporative cooling technology combines the thermally driven sorptive air dehumidification with indirect (Finocchiaro et al., 2012) or direct evaporative cooling to reduce the temperature of the supply air (White et al., 2009, Henning et al., 2001). Commercially available systems generally use desiccant rotors. There are disadvantages: The release of adsorption heat during the dehumidification process leads to a temperature increase in the sorption material, which significantly decreases the sorbents ability to adsorb moisture. This leads to decreased COP due to the alternating operation conditions between humidifying and dehumidifying the desiccant rotor (Bongs et al., 2014), which also prohibit the system from continuously supplying cooled and dehumidified air to the building. The latter can be solved by using two desiccant rotors in the system (Ge et al., 2010).

Bongs et al., 2014 investigated a desiccant cooling system with heat exchangers with silica gel and thermal cooling of the desiccant. The heat exchangers worked in staged mode, switching between adsorption mode and regeneration mode, enabling the system to continuously supply cooled and dehumidified air to the building.

Ge et al., 2010 compared the thermodynamic and economic performances of a solar driven two-stage rotary desiccant cooling system and a conventional vapor compression system in an office building located in Berlin and Shanghai. The authors showed that the desiccant cooling system could meet the cooling demand and provide comfortable supply air in both regions with required regeneration temperatures of 55 °C in Berlin and 85 °C in Shanghai. Compared to the vapor compression system, the desiccant cooling system had better supply air quality and consumed less electricity. Although, the initial investment cost of the solar cooling system was higher than for the conventional vapor compression system, the investment payback periods were only 4.7 years in Berlin and 7.2 years in Shanghai.

In general, absorption chillers have COP in the range of 0.4-0.85 for generator inlet temperature between 70 °C and 100 °C. They dominate the market. Adsorption chillers have COP in the range of 0.2-0.6, however, they can work at lower generating inlet temperatures in the range 45-65 °C (Ghafoor and Munir, 2015).

In this paper, a simple solar-driven open sorption system for comfort cooling with continuous supply of cooled and dehumidified air, no moving parts, operated at atmospheric pressure is investigated. The system only comprises an air solar collector with a desiccant layer, a cold storage with desiccant, fans powered by PV panels with a battery, a ventilation duct system with valves and a control system.

The solar air collector used for the present investigation is a modified version of an open-loop solar air collector from the company SolarVenti A/S. The air solar collector was developed in 2001. The solar air collector found a niche market among holiday homes where it primarily serves the purpose of keeping the building and the interior free of moisture outside the summer season. In this way, it protects the building and interior and preserves a dry and nice smelling indoor climate. The operation principle is simple: When the sun shines through the windows, the interior is heated. This releases moisture from the interior surfaces into the air. At the same time, a PV cell integrated into the air collector drives a ventilator that circulates heated air through the building. As heated air can absorb large amounts of moisture, the moisture is efficiently removed from the building. Additionally, the solar air collector contributes to the

heating of the house. Other areas where the company has successfully applied its product are garages, basements of year-round houses, storage buildings, ships, caravans, container buildings, and similar.

The solar air collector is covered with a polycarbonate cover plate which reduces the sensitivity of its operation to the presence of wind. The area of the solar air collector is 1.4 m^2. A photo and a principal drawing of the open-loop solar air collectors can be seen in Figure 1. The performance of the solar air collector was determined, in an outdoor test facility (Andersen, 2011). The measured solar air collector efficiencies are shown in Table 1.

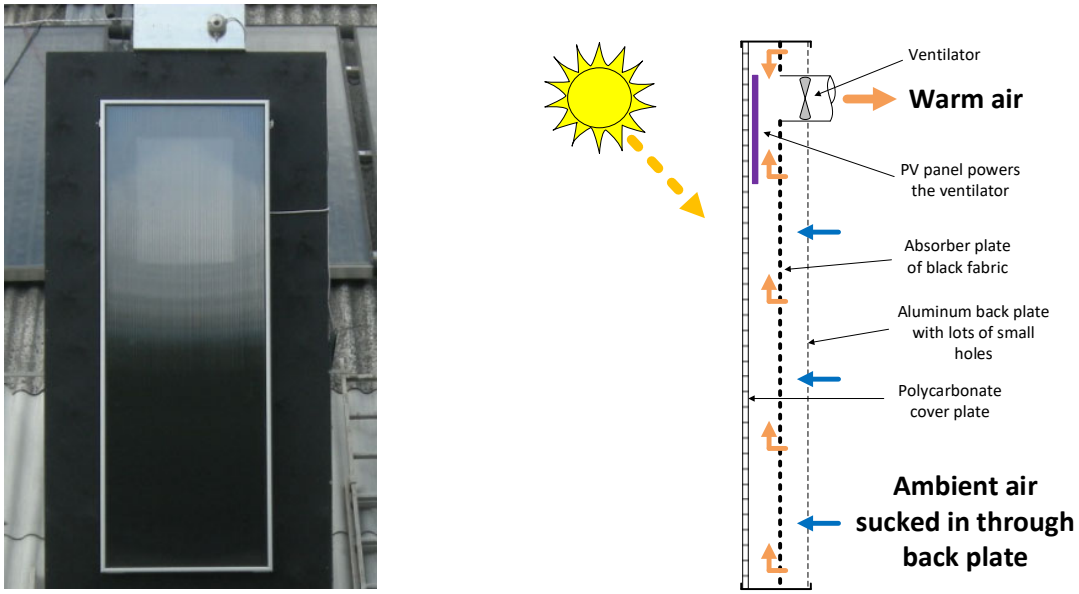

Figure 1. Photo of solar air collector from SolarVenti ApS (a) and principal drawing of the solar air collector (b).

Table 1: Measured efficiencies of the open-loop solar air collectors from Solar Venti ApS.

Air mass flow rate [kg/h/m^2]	(T_{outlet}-T_{amb})/G [(m^2·K)/W]	Efficiency [-]
128	0.0094	0.69
85	0.0126	0.61
83	0.0134	0.63
82	0.0125	0.58

To improve the dehumidification ability of the solar air collector, a layer of silica gel was added in the collector. Figure 2 shows the design and operation conditions of the solar dehumidifier. During the day, when the sun is shining the silica gel is dried out and then used to dehumidify the ventilation air during the night when air flows through the dry silica gel. At night, the ventilator is powered by electricity from the grid or a battery.

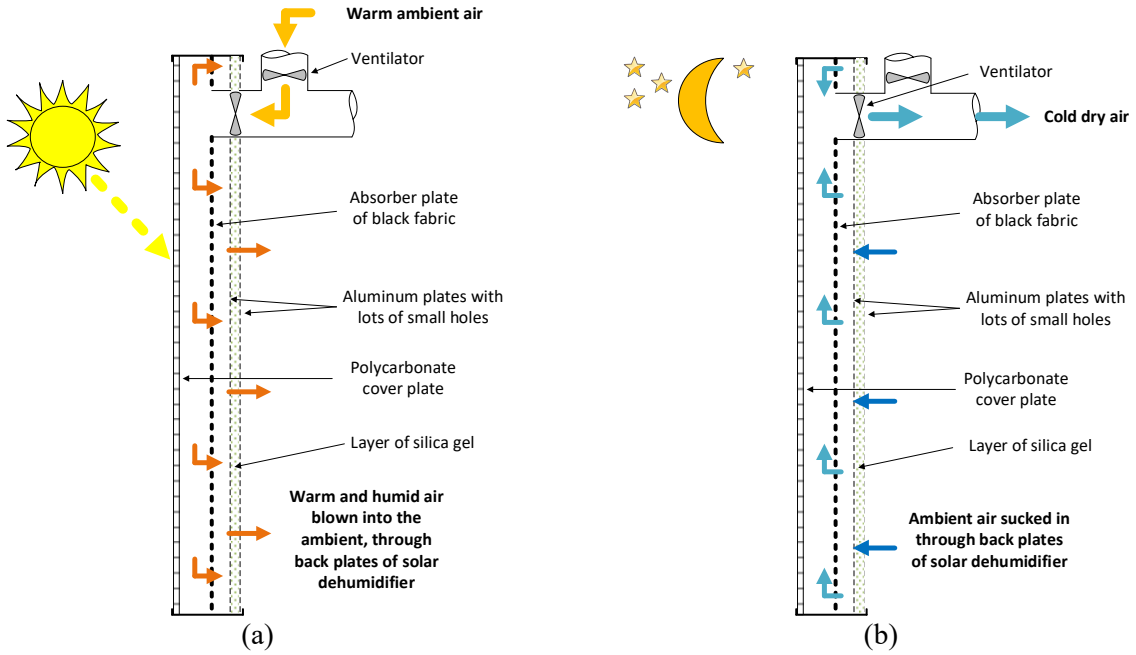

Figure 2: Principal drawing of the solar dehumidifier in charging mode (a) and discharging mode (b).

A proof of concept of the solar dehumidifier was performed in an outdoor test facility under real weather conditions (Andersen and Furbo, 2017). The thickness of the silica gel layer was 20 mm and the total mass of silica gel around 20 kg. The solar dehumidifier was installed on a south-facing surface with a tilt of 45°.

The tests showed that the silica gel was dried out best during the day with an airflow of around 100 m^3/h started when the solar radiation on the dehumidifier exceeded 600 W/m^2 and stopped when the solar radiation on the solar dehumidifier decreased below 500 W/m^2. The tests also show that the weight of the solar dehumidifier changed about 3.5 kg between day and night in the start of the test period. Later the weight change between day and night was reduced to about 2 kg.

Figure 3 shows measurements from three days at the beginning of the measurement period. Initially, the used control strategy operated the system in charge mode from sunrise to sunset and discharge mode from sunset to sunrise. The results clearly show that the desiccant layer in the solar dehumidifier starts adsorbing moisture at the end of the day, well before sunset.

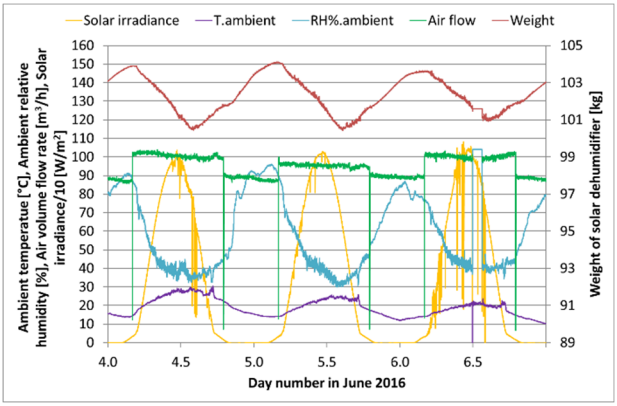

Figure 3: Measurements from the outdoor test of the solar dehumidifier.

2. Solar driven cooling system concept description

Motivated by the good performance of the solar dehumidifier, the solar-driven open sorption system for air comfort cooling in buildings was developed. The two main components of the system, the cold storage and the solar dehumidifier, both use a non-hazardous adsorption material and water vapor of an air stream as a working pair. Previous works (Neyer and Mugnier, 2018, Mugnier et al., 2017, Vasta et al., 2018, Grzebielec and Szelagowski, 2018, Rouhani, 2019) demonstrate that different storage types and principles can be used to store cold. Open adsorption systems with silica gel offer inexpensive and simple cold storage. Such systems combined with solar air collectors allow for solely solar-driven operation (Nielsen et al., 2019). The principle of the cooling system can be described as an open adsorption heat pump in intermittent operation, see Figure 4.

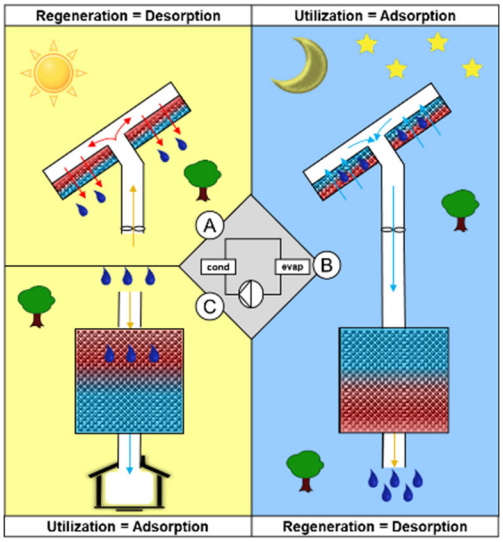

Figure 4: Principle diagram of cooling system

The solar air dehumidifier works as the thermal compressor, and the storage works as an alternating evaporator and condenser. The operation sequences work as follows:

A) During sunshine, ambient air is lead through the solar air dehumidifier, where it is heated before passing the implemented desiccant layer. With a flow rate of 100 m^3/h, air temperatures of typically, 50-60 °C are achieved, which allows the release of bound water (Andersen, 2011). The water vapor is released to the ambient. In this way, the solar air dehumidifier is dried.
B) During the nighttime, cool and humid air from ambient enters the solar air dehumidifier where the air is dried due to the implemented layer of desiccant. The dried, cool air stream is lead through the desiccant storage, where previously condensed water (C) evaporates into the air stream. As a consequence, the desiccant storage cools down. The driving force of this process is the partial water vapor pressure difference between the air volumes in the storage (high) and the inlet air stream (low). After several hours of operation, the storage dries and cools close to ambient (night) temperatures.
C) When cooling is needed, warm, humid ambient air (daytime) is ventilated through the cold desiccant storage, resulting in cooled and dried air for room ventilation.

In less sunny periods, the energy source for drying the desiccant in the solar dehumidifier can be energy from a PV powered battery or electricity from wind turbines. In this case, the solar dehumidifier must

have a built-in electrical heating surface. Alternatively, if excess heat from an industrial process is available, it can be used as well.

3. Theory

The cooling power supplied by the system is calculated from the ventilation air properties of temperature (t) and relative humidity (θ) measured at the inlet and outlet of the system. The measured values cannot be used directly, but must first be calculated into the absolute water content (x) and mass flow rate of dry air ($q_{air.dry}$). The calculations follow in equation 1-9.

The water content in the air (x) is calculated from the measured relative humidity (θ), the saturation pressure (p_{sat}) and the absolute atmospheric pressure (p) which is assumed constant at 101325 Pa (Peterson, F., 2000):

$$x = 0.622 \cdot \frac{\theta \cdot p_{sat}}{(p - \theta \cdot p_{sat})} \quad (1)$$

The saturation pressure (p_{sat}) is determined by the Antoine equation with the parameters A, B and C of 5.20389, 1733.926 and -39.48 respectively (Water (nist.gov), Bridgeman, 1964)

$$\mathrm{Log}_{10}(p_{sat}) = A - \frac{B}{(T+C)} \quad (2)$$

Equations 3-9 are used to calculate the cooling power (Peterson, F., 2000).

The density of moist air (ρ_{air}) is calculated by the water content (x) and the volume of 1 kg dry air (V):

$$\rho_{air} = \frac{(1+x)}{V} \quad (3)$$

The volume of 1 kg dry air (V) is calculated by the gas constant (R_0=8314.7 kJ/kmol/K) and the molar mass of dry air (M_{air}=28.97 kg/kmol), the temperature (T), the absolute atmospheric pressure (p), the relative humidity (θ) and the saturation pressure (p_{sat}):

$$V = \frac{8314.7 \cdot T \cdot 1}{28.97 \cdot (P - \theta \cdot p_{sat})} \quad (4)$$

The mass flow rate of moist air (q_{air}) is calculated by the density of moist air (ρ_{air}) and the measured volume flow rate ($v_{air.meas}$). The volume flow rate is measured in the center of the ventilation duct. An estimation of the real volume flow rate in the duct is made by assuming a parabola velocity distribution with zero velocity at the duct wall and the measured velocity as the maximum velocity in the duct. Thus, a multiplication factor of 0.67 is used:

$$q_{air} = \rho_{air} \cdot v_{air.meas} \cdot 0.67 \quad (5)$$

The fraction of dry air (f) in the moist air flow:

$$f = \frac{1}{(1+x)} \quad (6)$$

The mass flow rate of dry air ($q_{air.dry}$) is calculated by the fraction of dry air (f) and the mass flow rate of moist air (q_{air}):

$$q_{air.dry} = f \cdot q_{air} \quad (7)$$

The heat content of the moist air is calculated by the specific enthalpy (I) per kg dry air. 1.01 kJ/kg/K is the specific heat capacity of dry air, 2500 kJ/kg is the energy for vaporization of water at 0°C and 1.84 kJ/kg/K is the specific heat capacity of water vapor:

$$I = 1.01 \cdot t + x \cdot (2500 + 1.84 \cdot t) \quad (8)$$

Finally, the cooling power (P_{cool}) is calculated as the specific enthalpy difference of the air between in- and outlet of the storage:

$$P_{cool} = I_{inlet} \cdot q_{air.dry.inlet} - I_{outlet} \cdot q_{air.dry.outlet} \quad (9)$$

4. Material investigations

The choice of desiccant largely determines the cooling capacity of the open sorption system. A material investigation is undertaken to find the most suitable desiccant for both the solar dehumidifier and the cold storage. Five different silica gels and two zeolite types are investigated, see Table 2. Figure 5 to Figure 7 show photos of the investigated sorption material samples.

Silica gel has pores size much larger than the size of the adsorbed water molecules while zeolite has pore size approximately the same size as the absorbed water molecules. Consequently, the ultimate adsorption capacity of silica gel is usually higher than that of zeolite, at least at low temperatures. The larger pores of silica gel allow a continuous increasing in loading of adsorbed molecules with increased water vapor pressure. As the water vapor pressure increases, the regime of multilayer surface adsorption inside the pores merge into capillary condensation, which occurs in pores of ever-increasing diameter as the vapor pressure is raised. This relatively weaker bond between silica gel and water molecules means that less heat is released during adsorption in comparison to zeolites and, correspondingly, that desorption can occur at lower temperatures. Thus, silica gel is applicable where high adsorption capacity is required at low temperatures and moderate vapor pressure, and where heat of relatively low temperature is available for desorption. Therefore, silica gel is utilized as a desiccant in the open cycle systems (Boelman, 1995).

Table 2: Investigated sorption materials.

Sample number	Material description	Product information	Producer	Grain size
1	Silica gel, small porous, white, beads	PI-No.: SIO-02	Oker Chemie	1-3.15 mm
2	Silica gel, wide porous, beads	PI-No.: SIO-08	Oker Chemie	1.5-2.5 mm
3	Silica gel, small porous, white	Silica Gel White	ThoMar OHG	3-5 mm
4	Silica gel, wide porous, beige, beads 'FNG BEADS'	PI-No.: SIO-04	Oker Chemie	2-5 mm
5	Silica gel, small porous, white	PI-No.:SIO-01	Oker Chemie	3-6 mm
6	Zeolite Molecular sieve	Y	Chemiewerk Bad Köstriz	0.5-2 mm
7	Zeolite Molecular sieve	4A	SILKEM	3-5 mm

(1) Silica gel, small porous, white, beads (PI-No.: SIO-02)

(3) Silica gel, small porous, white (Silica Gel White)

(5) Silica gel, small porous, white (PI-No.:SIO-01)

Figure 5: Photos of investigated small porous silica gel materials.

(2) Silica gel, wide porous, beads (PI-No.: SIO-08)

(4) Silica gel, wide porous, beige, beads' FNG BEADS' (PI-No.: SIO-04)

Figure 6: Photos of investigated wide porous silica gel materials.

(6) Zeolite Molecular sieve (Y)

(7) Zeolite Molecular sieve (4A)

Figure 7: Photos of investigated zeolite materials.

The material samples are contained in 100 mm x 300 mm fabric bags that do not absorb moisture. This is crucial to ensure that moisture is only adsorbed in the sorption material. Furthermore, the bags are stitched to create paths that ensure an even distribution of the sorption material in the bags. The thicknesses of the prepared samples are around 20 mm.

4.1 Experimental set-up for material investigations

The investigation of the sorption materials is performed in a climate chamber in which temperature and relative humidity conditions can be accurately controlled separately, see Figure 8.

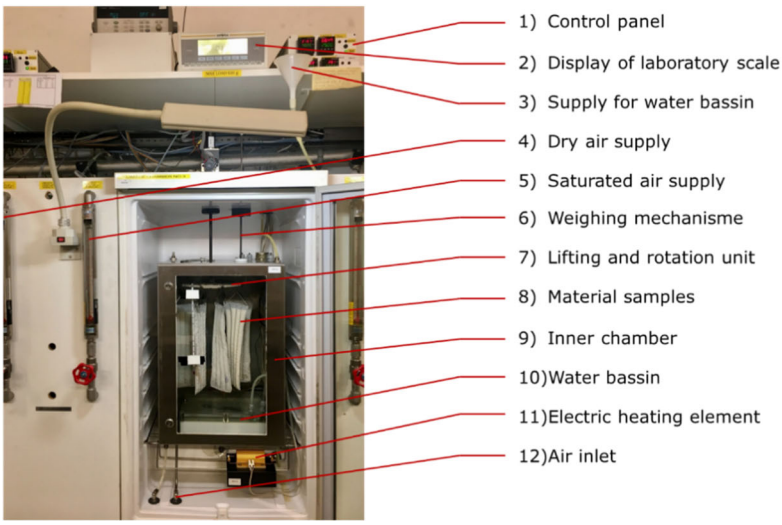

Figure 8: Set-up of the climate chamber.

The control panel (1) is used to set the desired temperature of the climate chamber and the water basin and the relative humidity. The laboratory-scale (2) monitors the weight of material samples during the automatic weighting cycles. The bags with the material samples (8) are hanged in a lifting and rotation unit (7). Throughout a weighing cycle, the bags are rotated and lifted. This unit is connected to the weighing mechanism (6) in which the bags hang freely in case of weighing. The purpose of the electric heating element (11) is to control the temperature in the outer climate chamber. A 'fine tuning' of the relative humidity and temperature in the inner climate chamber is realized through the water basin (10) that includes an additional heating element. To enhance the evaporation from the surface of the water basin, it is equipped with an air inlet for blowing bubbles in the water.

4.2 Test conditions for material investigations

Tests are carried out with conditions of temperature and relative humidity that resemble the conditions in the solar dehumidifier and the cold storage. For each setting of temperature and relative humidity, the tests are continued until a stable weight of the samples is reached.

Initially, the dry mass of the samples is determined by exposing the bags to a constant temperature of 105°C for a period of 24 h in an oven. Then, the sorption properties of the material samples are investigated at temperature levels of 20°C and 40°C. For each temperature level, the relative humidity is gradually increased from 20% to 80% and gradually decreased from 80% to 20%. Table 3 shows the absolute humidity for the applied test conditions in the climate chamber. Finally, cyclic tests are performed to resemble the conditions of temperature and relative humidity in the solar dehumidifier and the cold storage.

During the daytime, the sorbent in the solar dehumidifier is dried out. The ambient conditions are assumed to be warm and humid, with a temperature of 30°C and relative humidity of 45 %RH. It is further assumed that solar irradiance raises the temperature in the solar dehumidifier to 60°C. The air volume flow rate through the collector can be controlled to meet a specific temperature in the collector by altering the air volume flow rate or cyclic operation conditions. The warm air absorbs the moisture in the solar dehumidifier by evaporation. At the end of the day, the solar dehumidifier is dried out and the air that leaves the solar dehumidifier has the same absolute water content as the ambient air. Consequently, the investigated conditions of the air leaving the solar dehumidifier is a temperature of 60°C with a relative humidity of 10 %RH.

As well as the solar dehumidifier, the cold and dry storage is operated during the daytime. To investigate the cold storage performance, extreme ambient conditions of 30°C and 60 %RH are applied. By ventilating ambient air through the storage, it is cooled and dried out while the storage is gradually heated and humidified. The cooled, dry air can, for example, be used to condition buildings.

During the nighttime, the storage is charged with ambient air that has been dehumidified in the solar dehumidifier. The ambient conditions are assumed cold and humid with temperatures of 20°C and 25°C, and relative humidities of 80 %RH and 70 %RH, respectively. The air from the solar dehumidifier is sent to cool the storage at the corresponding temperature and low relative humidity, e.g. 10 %RH. During the charging process, the relative humidity of the ventilation air gradually increases as the solar dehumidifier humidifies. The investigated conditions of the air leaving the solar dehumidifier are 20°C with relative humidities of 10-30 %RH. Table 4 shows the sequential investigated climate conditions along with the absolute humidity at the specific climate conditions.

Table 3: Test conditions in the climate chamber.

Absolute humidity [g/kg]	20 %RH	40 %RH	60 %RH	80 %RH
20°C	2.9	5.8	8.7	11.7
40°C	9.2	18.7	28.4	38.5

Table 4: Test conditions in the climate chamber.

Solar dehumidifier			Cold storage		
Temperature [°C]	Relative humidity [%]	Absolute humidity [g/kg]	Temperature [°C]	Relative humidity [%]	Absolute humidity [g/kg]
20	80	11.7	30	60	16
60	10	12.5	20	30	4.3
20	80	11.7	30	60	16
60	10	12.5	20	20	2.9
25	70	13.9	30	60	16
60	10	12.5	20	10	1.4
25	70	13.9			

4.3 Results of material investigations

The results are shown as water uptake of the sorbent relative to the water uptake for the same sorbent at 20°C and 20 %RH as a function of the conditions of temperature and relative humidity in the climate chamber.

From Figure 9, it is clear to see that the silica gel materials have significantly higher water uptake than the zeolite materials in the investigated temperature and relative humidity levels. Further, the figure also shows that the small porous sorbents have a higher water uptake than the wide, porous sorbents for relative humidities up to 60 %RH and smaller water uptake than the wide, porous sorbents for relative humidities above 60 %RH. The different investigated grain size does not seem to influence the water uptake. It can also be seen that except for silica gel, sample 4, the kinetics of all material samples during adsorption are different from the kinetics during desorption at a relative humidity of 40 %RH for the silica gels. These kinetics indicate that the material samples are reluctant to rerelease the moisture.

Figure 10 shows the water uptake in the solar dehumidifier (a) and the storage (b) at the investigated conditions. It is evident that the solar dehumidifier humidifies and dries out at the applied operation conditions. At nighttime, while charging the cold storage, the solar dehumidifier has a water uptake of 20-25 % for the silica gels and 2-4 % for the zeolites. During the daytime, the solar dehumidifier rereleases the moisture. Further, it can be observed that the applied operation conditions result in identical kinetics in the cold storage, albeit the change in water uptake is not as pronounced in the storage as in the solar dehumidifier.

The investigated small porous silica gels, samples 1, 3, and 5 have very similar water uptake/release and are all good candidates for both the solar dehumidifier and the cold storage for this kind of application. The wide, porous silica gel, sample 2, is a suitable candidate as well. On the contrary, the wide, porous silica gel, sample 4 and the zeolites, samples 6 and 7, are not good candidates for this kind of application as the water uptake/release is too small.

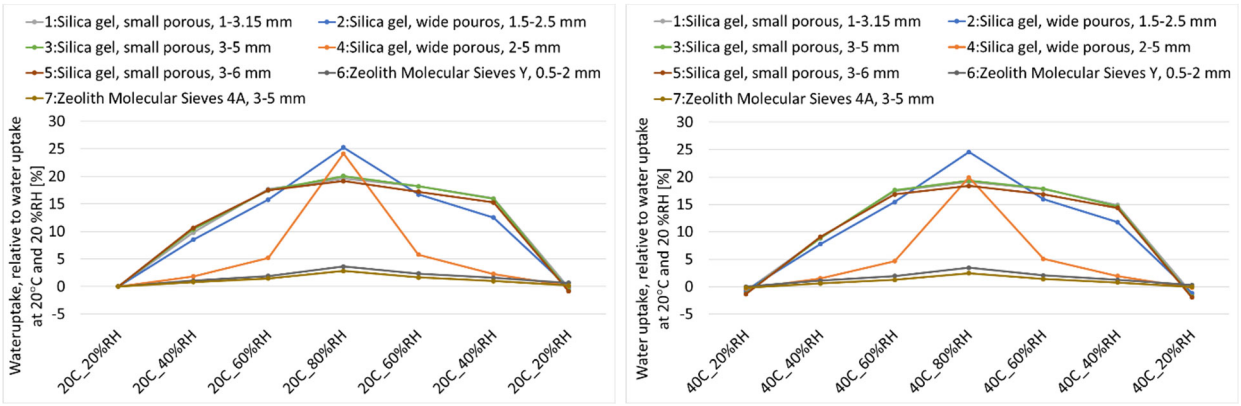

(a) (b)

Figure 9: Relative weight change at 20C (a) and 40C (b).

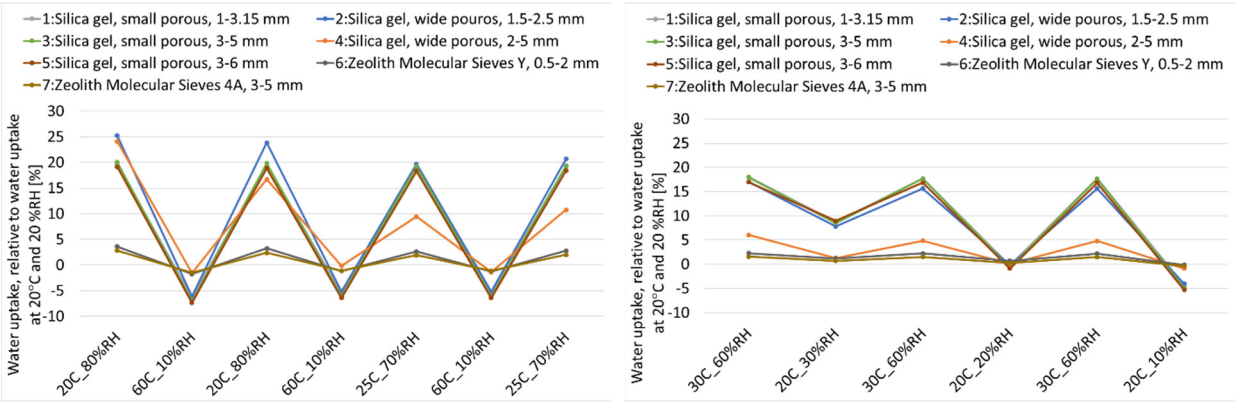

(a) (b)

Figure 10: Relative weight change at typical operating conditions in the solar dehumidifier (a) and the cold storage (b)

4.4 Comparison of material investigation results and manufacture specifications

To determine the absolute water uptake of the sorption materials in the climate chamber, a reference value for the dry mass of the samples is used.

Table 5 shows the water uptake relative to the dry sample weight from the investigations in the climate chamber. The results are very similar for the two applied temperature levels.

Table 6 shows the water uptake relative to the dry sample weight for all the investigated materials for which the manufacturer provides the information. The measurements from the climate chamber of sample 2 show a significant deviation from the manufacturer specification while the other samples meet the manufacturer specifications.

Table 5: Water uptake of dry samples, measured.

Sample	Dry sample weight [g]	Water uptake, relative to dry weight [%]							
		20 %RH		40 %RH		60 %RH		80 %RH	
		20°C	40°C	20°C	40°C	20°C	40°C	20°C	40°C
1	125.84	11.7	11.1	22.6	21.9	31.5	31.5	33.6	33.4
2	122.71	10.6	10.6	20	20.3	28	28.9	38.5	39.1
3	149.03	11.5	11.7	23	23.1	31	33.1	33.9	35
4	103.17	3.4	2.9	5.3	4.8	8.8	8.1	28.4	23.8
5	123.39	12.8	12.1	24.8	24	32.6	32.8	34.4	34.6
6	131.30	10.4	11.6	11.6	12.8	12.5	13.7	14.4	15.4
7	150.46	7.7	7.3	8.5	8.1	9.2	8.8	10.7	10.1

Table 6: Water uptake of dry samples, specified by the manufacturer.

Sample	Water uptake at 20°C, relative to dry weight [%]				
	20 %RH	40 %RH	50 %RH	80 %RH	100 %RH
1	≥10 %	≥21.5 %	-	≥31 %	-
2	-	-	-	≥60 %	≥70 %
3	≥10.5 %	-	≥23 %	≥34 %	-
4	-	-	-	-	-
5	≥10 %	≥20 %	-	≥31 %	-
6	-	-	-	-	-
7	-	-	-	-	-

5. Investigations of the solar-driven cooling system concept

Based on the results of the sorption material investigations, the small porous silica gel with a grain size of 3-5 mm from ThoMar OHG, sample 3 is used for full-scale investigations in both the solar dehumidifier and the cold storage. The air solar-driven open sorption system concept is constructed and tested in the indoor laboratory test facility.

5.1 Experimental set-up for system concept investigations

Figure 11 shows a schematic illustration and photos of the experimental set-up for the system test. The three main components are a storage tank, a loop to condition the airflow, and a solar dehumidifier. The cylindrical storage tank is made of plexiglass. It has an inner diameter of 0.4 m and a height of 0.8 m, resulting in a volume of 0.1 m^3, filled with 65 kg of silica gel. The loop is made of ventilation ducts with a diameter of 0.125 m. Both the storage tank and the loop are well insulated. The solar dehumidifier is not insulated, but a casing is mounted on the backside of the solar dehumidifier to control the temperature and humidity of the air volume flow rate through the solar dehumidifier. There is 20 kg of silica gel in the solar dehumidifier. In addition, the solar dehumidifier is equipped with heating wires, which are turned on

to imitate solar irradiance. The heating wires have a power of around 800 W, corresponding to an imitated utilized solar irradiance of 570 W/m^2.

The loop is operated by the ventilator, shown in Figure 12 (a). The ventilation air is first heated to the desired temperature by a heating element which is controlled by a PID controller, see Figure 12 (b). Then the water content of the air stream is conditioned by a humidifier. The humidifier is set to inject a defined amount of vapor into the air stream by evaporating water from a small container in the humidifier. When the water level in the container drops to a low level, freshwater is lead into the container to raise the water level again. During this short process, the humidifier cannot supply vapor to the air stream. Consequently, it is not possible to operate the system with constant relative humidity conditions when the evaporator is used. Further, the minimum amount of vapor produced by the evaporator is 1.2 kg/h, which restrain the set-up from meeting several specific operation conditions, e.g., night conditions with low temperature and high relative humidity. Consequently, these night conditions are approximated with an air stream that is conditioned to the desired temperature level but not humidified. After the vapor injection, the air and the vapor are mixed in long ventilation ducts before entering the system, see Figure 12 (c).

The temperature is measured in four different locations in the storage from top to bottom. Sensors measuring the relative humidity and the temperature are mounted in the ducts at the in- and outlet of the storage and the solar dehumidifier. A pressure transducer measures the pressure difference between the in- and outlet of the storage and weight cells measure the weight change of the storage. The air volume flow rate is measured in the center of the ventilation duct. The measurement equipment used in the experimental investigations of the system concept is listed in Table 7.

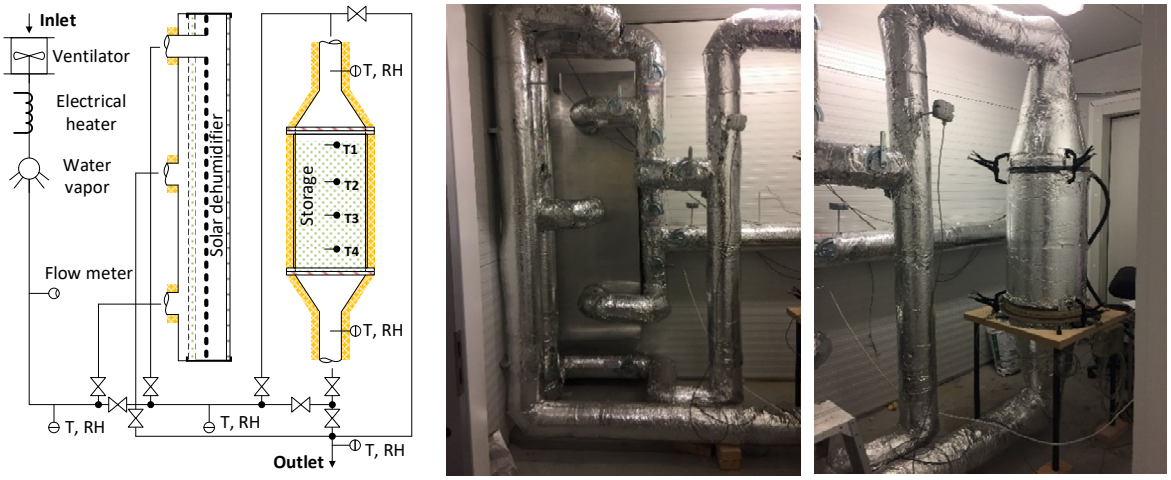

Figure 11: Experimental set-up for the system tests. (a) Schematic illustration. (b) Photo of the solar dehumidifier. (c) Photo of the storage tank.

(a) (b) (c) (d)

Figure 12: Experimental set-up for the system tests. Photo of the ventilator (a), the humidifier (b), ventilation ducts used to mix the air stream with the injected vapor (c) and the heating element and PID controller (d).

Table 7: Measurement equipment used in the system concept test.

Product information	Location	Type	Manufacturer	Accuracy
Temperature sensor	Cold storage	Copper/ constantan TT		0.5 K
Moisture and temperature sensor	Ventilation duct	EE 210	E+E Electronic Ges.m.b.H, Austria	≤90 %RH: ±(1.3+0.3 % of m. v.) %RH >90 %RH: ±2.3 %RH
Air volume flow meter	Ventilation duct	EE 650 (0.2-10 m/s)	E+E Electronic Ges.m.b.H, Austria	±(0.2 m/s+3 % of m. v.) m/s
Weight cell	Weight of storage	Z6(F/G)C3/50 kg	Mettler Toledo, Switzerland	±0.1 %
Pressure transducer	In/out cold storage	HUBA 699	Huba Control, Switzerland	±5 Pa (1.0 % of full scale)

5.2 Test conditions for the system concept tests

Figure 13 shows the air volume flow direction for charging the solar dehumidifier, discharging and charging the cold storage, respectively. The airflow direction through the cold storage is from top to bottom during discharge of the cold storage and from bottom to top during charging of the cold storage. This supports the natural flow direction since the ventilation air is dehumidified during discharge of the cold storage resulting in increasing its specific weight, whereas it is humidified during the charge of the cold storage and hence becoming lighter. Further, the applied flow direction prevents re-humidification and re-dehumidification of the ventilation air, caused by the moisture gradient, as it passes through the part of the storage that has not yet been activated.

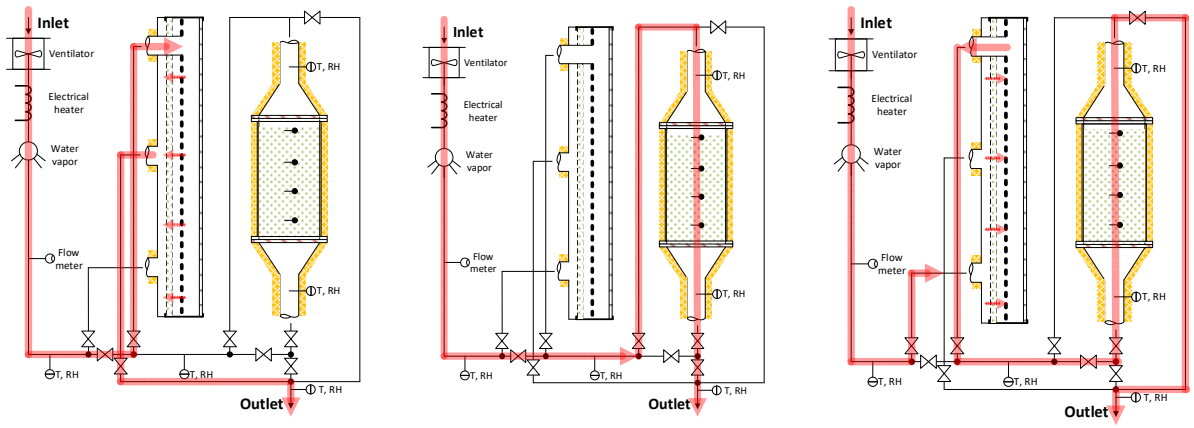

(a) (b) (b)

Figure 13: Airflow direction. (a) Charging the solar dehumidifier during the daytime. (b) Discharging the storage during the daytime. (c) Charging the storage during nighttime.

The applied operation conditions for the cyclic tests are listed in Table 8 to Table 10. The operation conditions are not constant during the tests and the shown values in the tables are average values. The tests are referred to as test 1, test 2, and test 3.

Table 8: Operation conditions in test 1.

Test 1	Operation mode	Air volume flow rate [m^3/h]	Temperature in [°C]	Relative humidity in [%]	Temperature out [°C]	Relative humidity out [%]
1A	Charge solar dehumidifier	75	32	46	50	23
1B	Discharge storage	40	31	73	14	37
1C	Discharge solar dehumidifier	40	16	40	19	22
1D	Charge storage	40	19	22	22	43

Table 9: Operation conditions in test 2.

Test 2	Operation mode	Air volume flow rate [m3/h]	Temperature in [°C]	Relative humidity in [%]	Temperature out [°C]	Relative humidity out [%]
2A	Charge solar dehumidifier	55	32	56	52	25
2B	Discharge storage	56	31	60	20	15
2C	Discharge solar dehumidifier	57	16	36	20	20
2D	Charge storage	57	20	20	21	41

Table 10: Operation conditions in test 3.

Test 3	Operation mode	Air volume flow rate [m3/h]	Temperature in [°C]	Relative humidity in [%]	Temperature out [°C]	Relative humidity out [%]
3A	Charge solar dehumidifier	43	32	67	53	29

3B	Discharge storage	40	30	78	18	23
3C	Discharge solar dehumidifier	41	18	36	21	20
3D	Charge storage	41	21	20	22	44

5.3 Results of the system concept tests

The temperatures in the sorption storage during discharge and charge are shown in Figure 14 - Figure 16.

At the time of the test sequences 1, the total weight of the storage tank varies between 108 and 109 kg. The silica gel is relatively dry and from Figure 14 is can be observed heat released during adsorption is stronger in the middle part of the storage where the silica gel is dryer than in the top and the bottom of the storage. Is can also be observed that the adsorption takes place layer by layer from the top to the bottom of the storage. Regardless of the very high storage temperatures, the ventilation air circulated through the storage cools effectively.

At the time of the test sequences 2 and 3, se Figure 15 - Figure 16 the total weight of the storage varies between 112 and 113 kg. The silica gel in the storage has adsorbed 4 kg of moisture more than in test 1. Due to the higher water content in the storage, the heat release during sorption has decreases, and so has the temperature cooling of the ventilation air circulated through the storage.

The discharging and charging times are similar in the experiments with similar operation conditions regardless of the saturation levels of the storage.

Charging and discharging happens sequentially. This indicates that the shape of the storage is not important and storage for example could be integrated into a wall in the building.

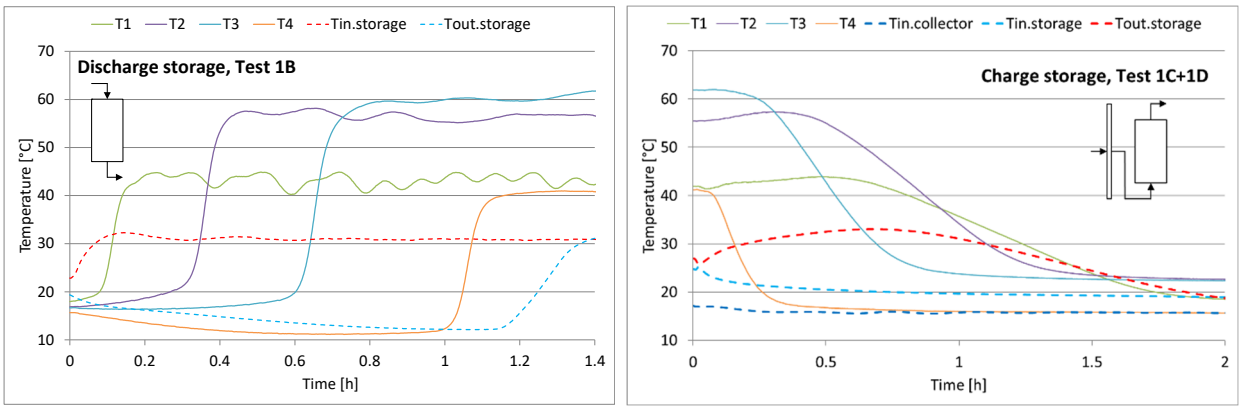

(a) (b)

Figure 14: Inlet, outlet and storage temperatures during discharge (a) and charge (b) in test 1.

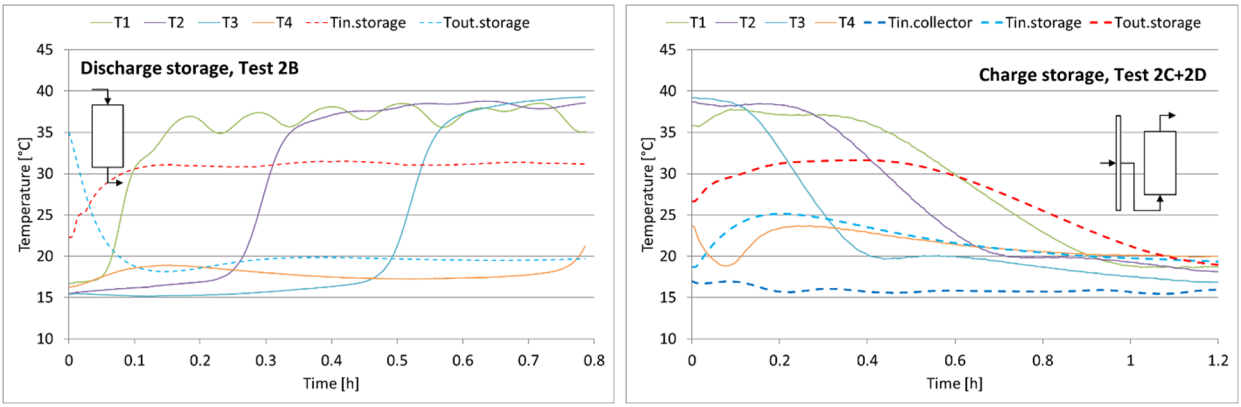

(a) (b)

Figure 15: Inlet, outlet and storage temperatures during discharge (a) and charge (b) in test 2.

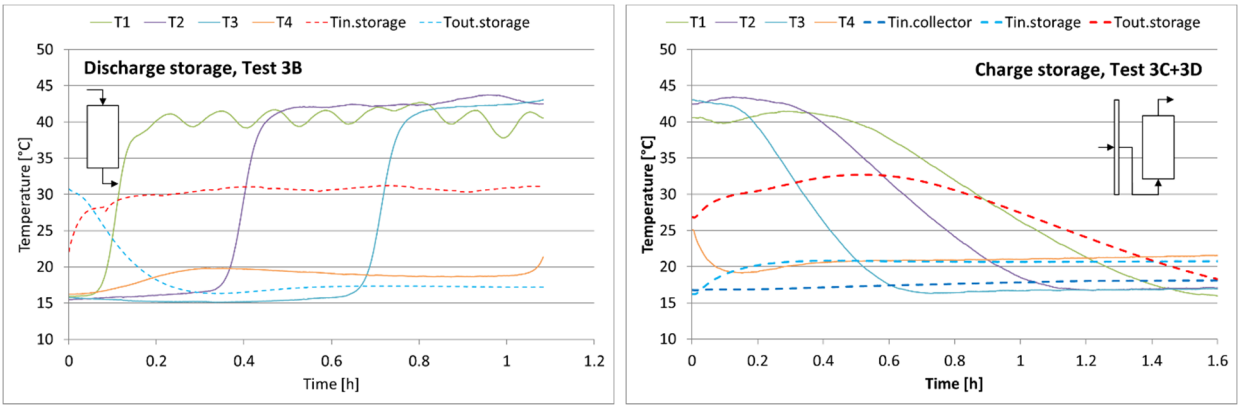

(a) (b)

Figure 16: Inlet, outlet and storage temperatures during discharge (a) and charge (b) in test 3.

Figure 17 shows the temperatures and relative humidities at the in- and outlet of the solar dehumidifier during charging of the solar dehumidifier. The solar dehumidifier reaches stable conditions within 2-3 hours.

Figure 18 shows the temperatures and relative humidities at the in- and outlet of cold storage during discharging. Next to that, the figure displays the pressure drop in the cold storage. In test 1, the average moisture contents in the in- and outlet ventilation air are around 21 g/kg and 4 g/kg, respectively, corresponding to a change in water content of around 17 g/kg. In test 2, the average moisture contents in the in- and outlet ventilation air are around 17 g/kg and 2 g/kg, respectively, corresponding to a change in water content of around 15 g/kg. In test 3 with similar operation conditions as test 1, the average moisture contents in the in- and outlet ventilation air are around 21 g/kg and 3 g/kg, respectively, corresponding to a change in water content of around 18 g/kg. The results show that, although the saturation level of the storage is higher in test 3 than in test 1, the storage still works effectively.

The air volume flow rate in test 1 and 3 is around 40 m^3/h while test 2 is performed with an air volume flow rate of around 60 m^3/h. The increase in air volume flow rate directly impacts the pressure drop in the storage. For the low air volume flow rate, the pressure drop is around 270 Pa, whereas the high air volume flow yields around 370 Pa.

Figure 19 shows the temperature decrease in the ventilation air circulated through the storage and corresponding power discharge from the cold storage. The average power discharge is 753, 820, and 720 W in tests 1, 2, and 3, respectively.

Figure 20 shows the temperatures and relative humidities at the in- and outlet of the solar dehumidifier during discharging of the solar dehumidifier and charging of the cold storage. Note that the outlet from the solar dehumidifier is equal to the inlet to the cold storage. The outlet temperatures from the solar dehumidifier are higher than the inlet temperatures to the solar dehumidifier. This results from the adsorption process in the solar dehumidifier that comes along with the release of heat. Due to the indoor location of the solar dehumidifier and the casing mounted on its backside, the temperature increase in the component is more significant than it will be in the real application, where the solar humidifier is located outside of the building.

Figure 21 and Figure 22 show the water uptake during the discharging and charging cycles for the three tests. Both the directly measured water uptake and the water uptake calculated using the measured temperatures and relative humidities are shown. It can be seen that there is a high degree of similarity between the measured and calculated water uptake in the cold storage. Further, the water uptake while discharging the storage is similar to the water release during charging of the cold storage. The weight of the solar dehumidifier is not measured. Consequently, only the calculated water uptake is shown. It can be seen that the water uptake in the solar dehumidifier is much lower than the water release in the storage during the charging tests. The reason is that the mass of silica gel in the solar dehumidifier is lower than the mass of silica gel in the storage.

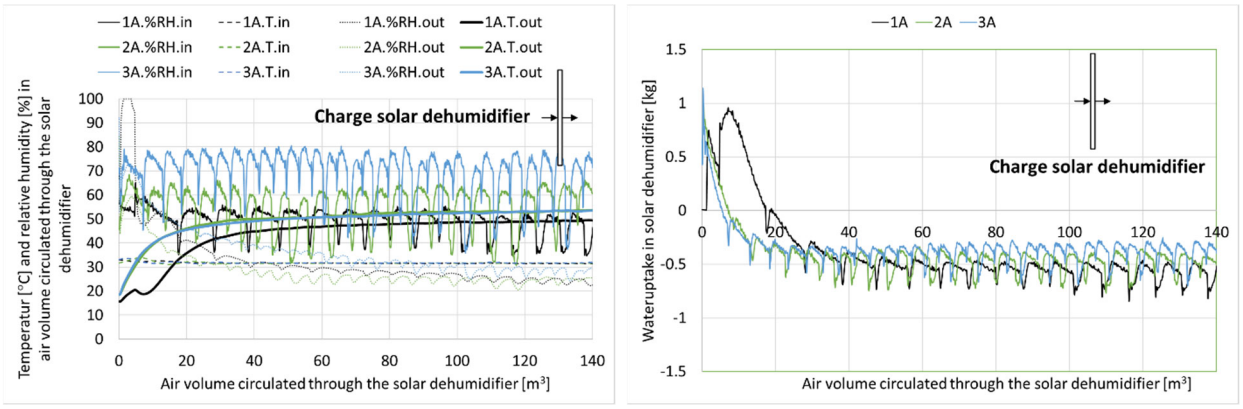

(a) (b)

Figure 17: Operation conditions (a) and water uptake (b) in the solar dehumidifier during charging.

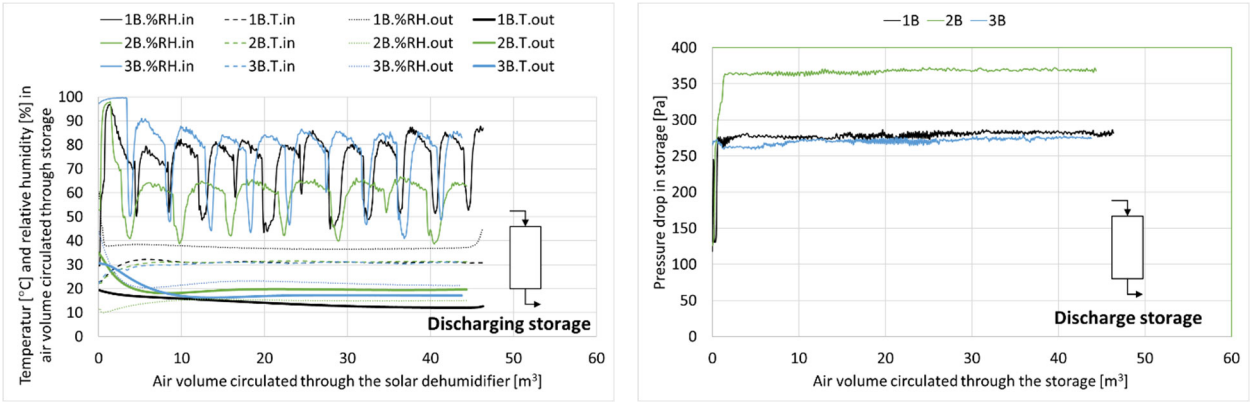

(a) (b)

Figure 18: Operation conditions (a) and pressure drop in storage (b) during discharging of the cold storage.

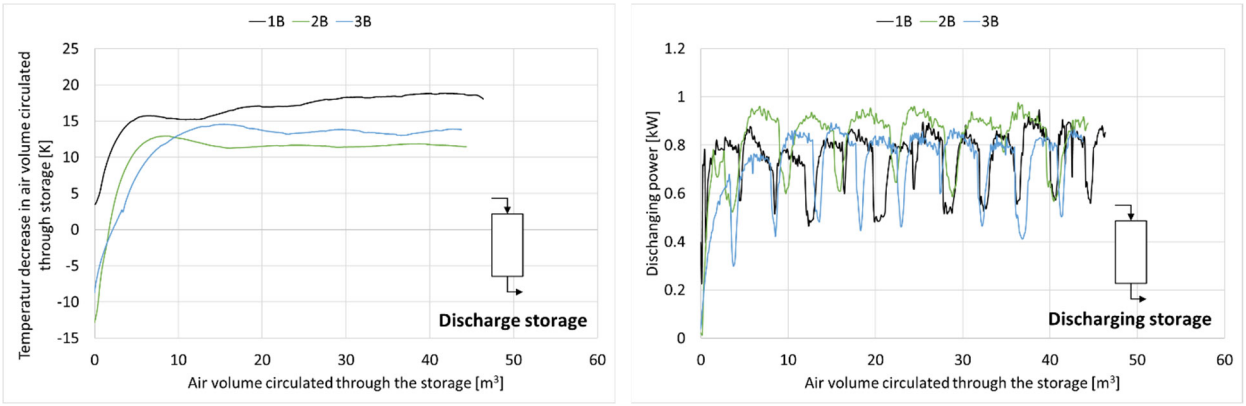

(a) (b)

Figure 19: Temperature drop in ventilation air (a) and the discharging power (b) during discharging the cold storage.

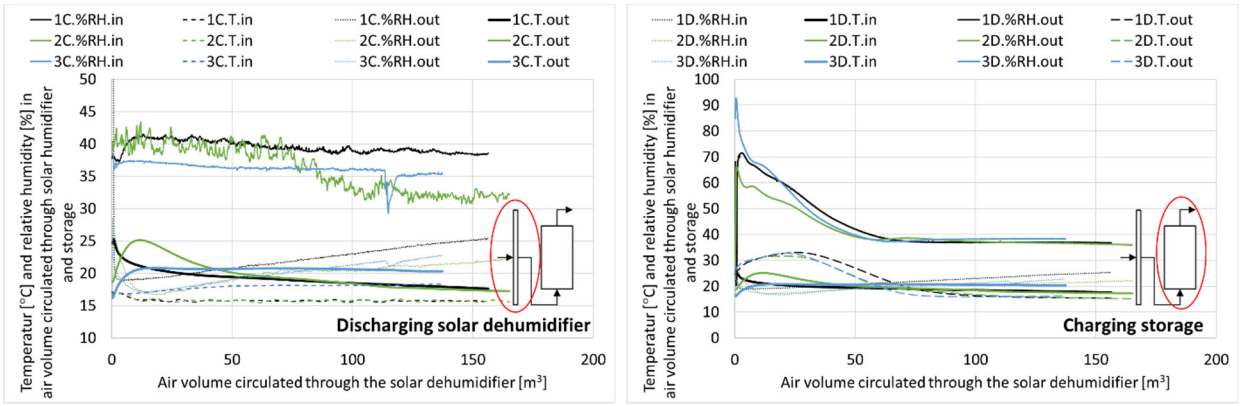

(a) (b)

Figure 20: Operation conditions during discharge of solar dehumidifier (a) and charge of cold storage (b).

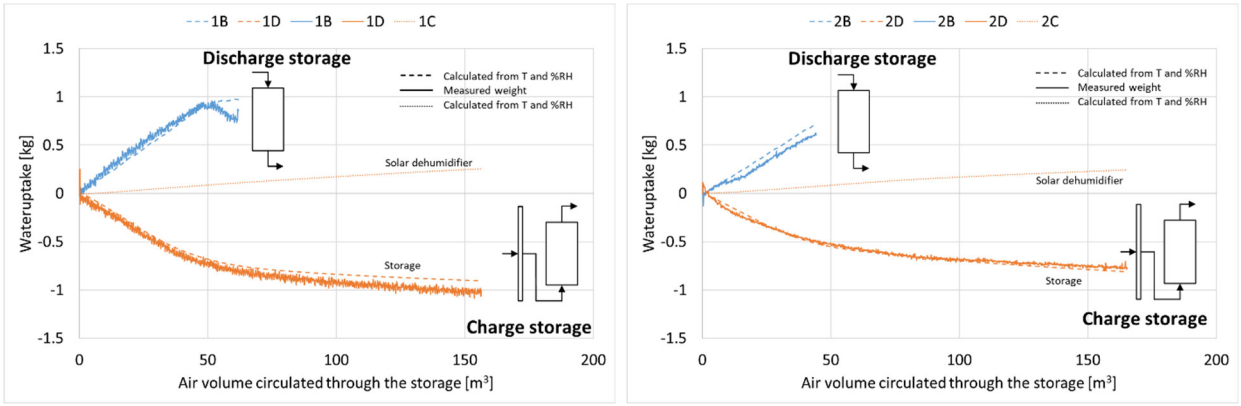

(a) (b)

Figure 21: Water uptake in cold storage and solar dehumidifier during discharging and charging the storage for test 1 (a) and test 2 (b).

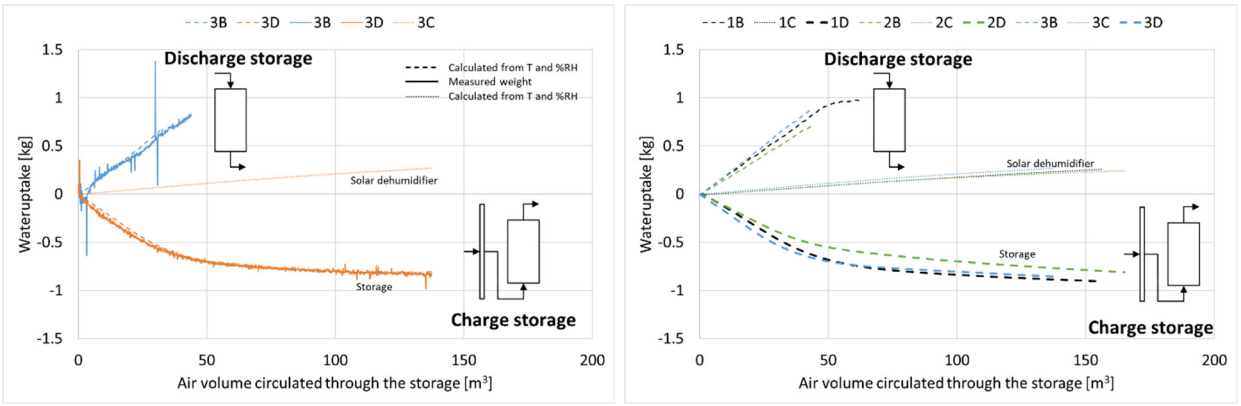

(a) (b)

Figure 22: Water uptake in cold storage and solar dehumidifier during discharging and charging the storage for test 2 (a) and test 1, 2, and 3 (b).

6. Potential for the technology

Unlike compression or absorption chillers, the operation of a solar-driven open-sorption cooling system is limited by ambient conditions. The potential of the system is addressed by investigating the climatic conditions of fourteen different locations, see Table 11. The majority of the listed locations lie within the Sunbelt region between latitude 40° North and 40° South. The details of the investigated locations are derived from the simulation program Polysun (Vela Solaris AG, 2021). The program uses climate data from meteonorm (Meteonorm, 2020).

Table 11: Details of investigated locations.

Location	Latitude [°]	Longitude [°]	Elevation [m]	Collector tilt [°]	Solar radiation on collector [kWh/(m^2·y)]
Copenhagen, Denmark	55.72	12.57	19	41	1237
Munich, Germany	48.13	11.58	536	38	1387
Beijing, China	39.93	116.4	30	36	1582
Melbourne, Australia	-37.75	144.97	82	30	1725
Orlando, USA	28.43	-81.32	32	24	1755
Palermo, Italy	38.1	13.38	1	34	1798
Auckland, New Zealand	-36.92	174.6	32	32	1802
Rio de Janeiro, Brazil	-22.88	-43.28	152	20	1858
New Delhi, India	28.62	77.22	213	28	1985
Heraklion, Greece	35.32	25.13	40	28	1996
Lisbon, Portugal	38.72	-9.15	77	34	2036
Seville, Spain	37.23	-5.98	17	32	2086
Dubai, United Arab Emirates	25.23	55.28	0	24	2149
Johannesburg, South Africa	-26.17	28.03	1676	26	2451

The following assumptions are used for a simplified investigation of the potential of the technology for the different locations:

- A building with heat loss coefficient of 150 W/K
- Area of one solar dehumidifier is 1.4 m^2
- Cooling capacity of the sorption storage is 0.75 kWh per 65 kg silica gel
- Ratio between area of solar dehumidifier and sorption storage volume is constant
- Cooling demand if ambient temperature t > 26 °C
- Cooling demand is determined by hourly values as (t-26) K·150 W/K
- Charging of solar dehumidifier is only possible when solar irradiance onto the solar dehumidifier > 500 W/m^2. That means neglecting the solar dehumidifier performance for lower solar irradiances in spite of the fact that a more advanced control system with variable flow rate allows performance even for low solar irradiances.

The daily values of solar energy onto the solar dehumidifier, the storage cooling capacity when fully charged, and the cooling demand of the building are compared. The yearly system cooling performance is then determined as the sum of the lowest daily value of the three values.

3.1 Results of climate investigations

Figure 23 shows the number of days per year where the maximum ambient temperature exceeds a defined ambient temperature. The figure also shows the fraction.demand, which is defined as the number of days with Tamb.max > 26 °C in a defined number of hours relative to the number of days with Tamb.max > 26 °C. Thus, the figure indicates the number of hours with comfort cooling demand on days with comfort cooling demand in the different climates.

Figure 24 shows the yearly cooling demand for all the locations and the system cooling performance to the area of the solar dehumidifier. Without assistance of any supplementary energy for drying the solar dehumidifier, the cooling demand can be covered in Copenhagen, Palermo, Auckland, Heraklion, Lisbon, Seville, Dubai and Johannesburg with an appropriate system size.

For the locations of Munich, Beijing, Melbourne, Orlando, Rio de Janeiro and New Delhi, the lack of coincidence between cooling demand and solar irradiance make the technology less promising.

The investigations show that the potential for the technology is highest in Dubai.

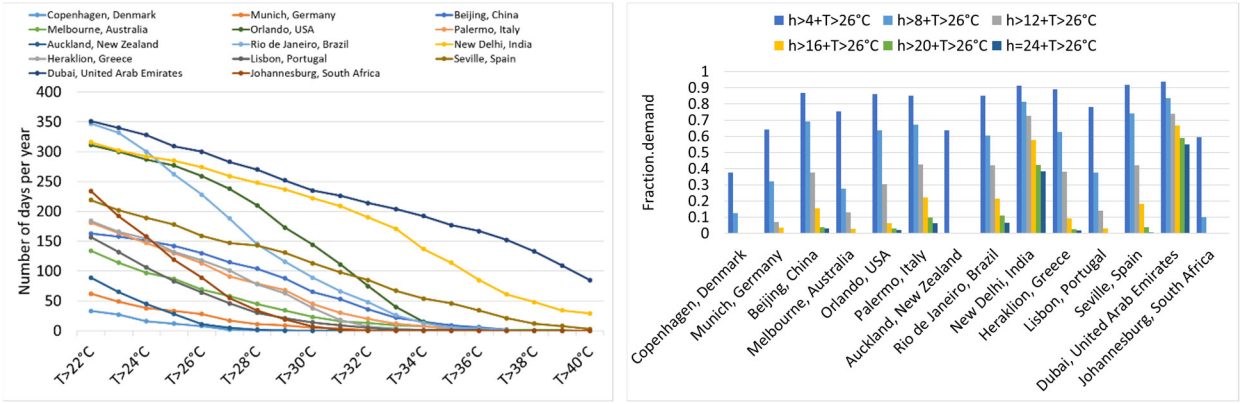

(a) (b)

Figure 23: Climate characteristics of different locations. (a): Number of days with Tamb.max.>defined temperature. (b): Fraction: number of days with Tamb.max>26°C in a defined number of hours relative to number of days with Tamb.max>26°C.

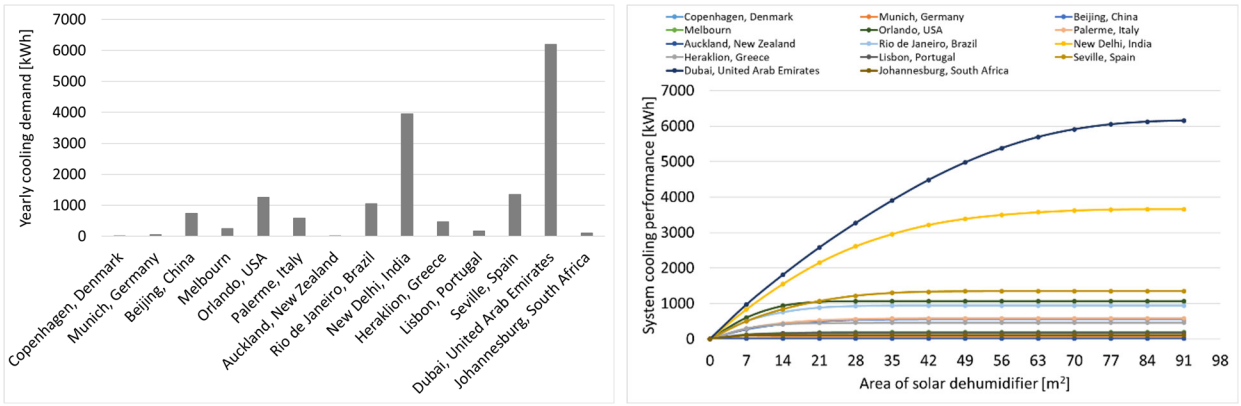

(a) (b)

Figure 24: Cooling demand (a) and system cooling performance (b).

7. Conclusions and outlook

An air solar-driven open-loop sorption system for air comfort cooling in buildings is tested in an indoor laboratory test facility.

The cooling system contains two main components: The solar air dehumidifier and the cold storage with desiccant. An investigation of different desiccant materials, including both small and wide porous silica gels as well as synthetic zeolites, reveals that a small porous silica gel is the best option for desiccant in both the solar dehumidifier and the cold storage. The investigation of desiccant materials is performed in a climate chamber where temperature and relative humidity can be set very accurately.

The investigations of the cooling system show that the temperature of the ventilation air circulated through the charged cold storage is reduced by 11 K-19 K, depending on the operation conditions. Not only the ventilation air temperature is lower in the cold storage, but also the relative humidity is lowered. Thus, the system can supply cool dry air for comfort cooling of buildings. The measured cooling power of the system is 800-900 W. The investigations also show that the saturation level in the cold storage does not influence the performance significantly, as long as the cold storage is not fully saturated. In one cycle, the amount of moisture adsorbed in the storage during discharge is removed again during charging of the cold store. The discharge period is shorter than the charge period of the cold storage. The pressure drop over the cold storage is measured to 270 Pa and 370 Pa with air volume flow rates of 40 m^3/h and 60 m^3/h, respectively. The pressure drop over the cold storage is not affected by the saturation level of the cold storage.

A climate investigation, including fourteen different climates, mainly from the Sunbelt region, reveals that the solar cooling system can work well in eight of the investigated climates.

Based on the promising results of the investigations, it is recommended to:

- Work out design, planning, and optimization tools for the system to be used for different climates.
- Demonstrate the system's performance, costs, and reliability in practice.

Funding

The work was supported by the Danish Bjarne Saxhof foundation.

Nomenclature

G	Solar irradiance on a tilted surface (W/m^2)
h	Time (h)
I	Specific enthalpy (kJ/kg)
M	Molar mass (kg/kmol)
P	Power (kJ/h)
p	Atmospheric pressure (Pa)
q	Mass flow rate (kg/h)
R_0	Gas constant (kJ/kmol/K)
T	Temperature (K)
t	Temperature (°C)
V	Volume (m^3)
v	Volume flow rate (m^3/h)
x	Water content (kg/kg)

Non-dimensional quantities

Fraction	Fraction
f	Fraction of dry air

Symbols

θ	Relative humidity (%)
ρ	Density (kg/m^3)

Subscripts

air	Atmospheric air
amb	Ambient
cool	Cooling
demand	Demand
dry	Dry air
inlet	Inlet
max	Maximum
meas	Measured
outlet	Outlet
sat	Saturated
t	Total

References

Abdulateef, J.M., Sopian, K., Alghoul, M.A., Sulaiman, M.Y., 2009. Review on solar-driven ejector refrigeration technologies. Renewable and Sustainable Energy Reviews 13, pp. 1338-1349

Andersen, E., 2011. Solar Air Collector Test Facility (in Danish). Technical University of Denmark, DTU Byg R-255, http://www.byg.dtu.dk/Forskning/hentned.aspx

Andersen, E., Furbo, S., 2017. Solar Dehumidifier (in Danish). Technical University of Denmark, DTU Byg R-368, http://www.byg.dtu.dk/Forskning/hentned.aspx

Boelman, E.C., Saha, B.B., Kashiwagi, T., 1995. Experimental investigations of a silica gel-water adsorption refrigeration cycle-The influence of operation conditions on cooling output and COP, Ashrea Transactions, Volume 101, pp. 358-366

Bongs, C., Morgenstern, A., Lukito, Y., Henning, H.M., 2014. Advanced performance of an open desiccant cycle with internal evaporative cooling. Solar Energy 104, pp. 103-114

Boopathi, V.R, Shanmugam, V.A., 2012. A review and new approach to minimize the cost of solar assisted absorption cooling system. Renew Sustain Energy Rev. 16, pp. 6725-6731

Bridgeman, O.C., Aldrich, E.W., 1964. Vapor Pressure Tables for Water**.** J. Heat Transfer 86, 2, pp. 279-286, https://doi.org/10.1115/1.3687121

Finocchiaro, P., Beccali, M., Nocke, B., 2012. Advanced solar assisted desiccant and evaporative cooling system equipped with heat exchangers. Solar Energy 86, pp. 608-618

Ge, T.S., Ziegler, F., Wang, R.Z., Wang, H., 2010. Performance comparison between a solar driven rotary desiccant cooling system and conventional vapor compression system (performance study of desiccant cooling). Applied Thermal Engineering 30, pp. 724-731

Ghafoor, A., Munir, A., 2015. Worldwide overview of solar thermal cooling technologies. Renewable and Sustainable Energy Reviews 43, pp. 763-774

Grignon-Masse, L., Riviere, P., Adnot, J., 2011. Strategies for reducing the environmental impacts of room air conditioners in Europe, Energy Policy 39, pp. 2152-2164

Grossman, G., 2002. Solar-powered systems for cooling, dehumidification and air conditioning. Solar Energy 72, pp. 53-62

Grzebielec, A., Szelągowski, A., 2019. Experimental study of a sorption cold storage supporting the air conditioning system. Modern Engineering vol 1, pp. 10-15

Henning, H.-M., Erpenbeck, T., Hindenburg, C., Santamaria, I.S., 2001. The potential of solar energy use in desiccant cooling cycles. Int. J. Refrig 24, pp. 220-229

IEA, International Energy Agency, 2012. Technology Roadmap, Solar Heating and Cooling: Technology Roadmap - Solar Heating and Cooling – Analysis - IEA

Jakob, U., 2020. IEA SHC Task 65 – Solar Cooling for the Sunbelt Regions, 2020 Highlights: IEA SHC || Task 65 || Publications (iea-shc.org)

Kalkan, N., Young, E.A., Celiktas, A., 2012. Solar thermal air conditioning technology reducing the footpring of solar thermal air conditioning. Renew Sustain Energy 16, pp. 6352-6383

Meteonorm 8 Softwate, 2020. www.meteonorm.com

Mugnier, D., Neyer, D., White, S.D., 2017. The Solar Cooling Design Guide: Case Studies of Successful Solar Air Conditioning Design. IEA SHC Task 53. Wiley, Ernst & Sohn, ISBN 10 3433031258

National Institute of Standards and Technology, NIST Chemestry WebBook, SRD 69, U.S. Department of Commerce Water (nist.gov)

Neyer, D., Mugnier, D., 2018. New Generation Solar Cooling & Heating Systems - PV or solar thermally driven systems. Solar Heating and Cooling & Solar Air-Conditioning Technology Position Paper.

Nielsen, E., Englmair, G., Furbo, S., 2019. An open Sorption System for Solar Air Cooling in Buildings. ISES Solar World Congress 2019 and IEA SHC conference 2019, Santiago, Chile.

Oke, T.R., Johnson, G.T., Steyn, D.G., Watson, I.D., 1991. Simulation of surface urban heat islands under 'ideal' conditions at night, 2. Diagnosis of causation, Boundary layer Meteorology 56(4), pp. 339-358

Peterson, F., 2000. Psychrometri och luftbehandling, Kompendium II:2 (third revisied edition), Uppvärmnings- och ventilationsteknik, KTH, Stocholm.

Pons, M., Anies, G., Boudehenn, F., Bourdoukan, P., Castaing-Lasvignottes, J., Evola, G., Le Denn, A., Le Pierrès, N., Marc, O., Mazet, N., Stitou, D., Lucas, F., 2012, Performance comparison of six solar-powered air conditioners operated in five places, Energy 46, pp. 471-483

Rouhani, M., 2019. Sorption thermal energy storage for sustainable heating and cooling. PhD report, etd20484, Simon Fraser University, Canada.

Santamouris, M., Papanikolaou, N., Livada, I., Koronakis, I., Georgakis, C., Argiriou, A., et al., 2001. On the impact of urban climate on the energy consumption of buildings. Solar Energy 70, pp. 201-216

Vasta, S., Brancato, V., La Rosa, D., Palomba, V., Restuccia, G., Sapienza, A., Frazzica, A., 2018. Nanomaterials Adsorption Heat Storage: State-of-the-Art and Future Perspectives. Nanomaterials, vol 8(7), pp. 522

Vela Solaris AG, 2021. Polysun 12.0.10, https://www.velasolaris.com/downloads/?lang=en

White, S.D., Kohlenbach, P., Bongs, C., 2009. Indoor temperature variations resulting from solar desiccant cooling in buildings without thermal backup. Int. J. Refrig. 32, pp. 695-704

Yu, N., Wang, R.Z., Wang, L.W., 2013. Sorption thermal storage for solar energy. Progress in Energy and Combustion Science 39, pp. 489-514